



Universidad Autónoma
de Madrid

Biblos-e Archivo
Repositorio Institucional UAM

Repositorio Institucional de la Universidad Autónoma de Madrid

<https://repositorio.uam.es>

Esta es la **versión de autor** del artículo publicado en:

This is an **author produced version** of a paper published in:

Chemical Engineering Journal 371 (2019): 868-875

DOI: <https://doi.org/10.1016/j.cej.2019.04.138>

Copyright: © 2019 Elsevier B.V. This manuscript version is made available under the CC-BY-NC-ND 4.0 licence <http://creativecommons.org/licenses/by-nc-nd/4.0/>

El acceso a la versión del editor puede requerir la suscripción del recurso

Access to the published version may require subscription

**Adsorption of ibuprofen on organo-sepiolite and on zeolite/sepiolite heterostructure:
Synthesis, characterization and statistical physics modeling**

Zichao Li ^a, A. Gómez-Avilés^b, Lotfi Sellaoui^{c*}, Jorge Bedia^b, Adrián Bonilla-Petriciolet^d,
Carolina Belver^{b**}

^a Research Institute of Advanced Interdisciplinary, College of Life Sciences, Qingdao
University, Qingdao 266071, China

^b Sección de Ingeniería Química, Facultad de Ciencias, Universidad Autónoma de Madrid, C/
Francisco Tomas y Valiente 7, 28924 Madrid, Spain

^c Laboratory of Quantum and Statistical Physics, LR18ES18, Monastir University, Faculty of
Sciences of Monastir, Tunisia

^d Instituto Tecnológico de Aguascalientes, Aguascalientes, 20256, Mexico

Corresponding Authors: sellaouilotfi@yahoo.fr (* Lotfi Sellaoui)

carolina.belver@uam.es (** Carolina Belver)

Abstract

A synthesized zeolite/sepiolite nanoheterostructure (Zeo-Sep) and a modified organo-sepiolite (O-Sep) have been employed as clay-based adsorbents to study the adsorption mechanism of ibuprofen (IBP) from aqueous solution. New equilibrium data of IBP adsorption were determined at 20 – 60° C, which were utilized to perform a theoretical analysis of the removal mechanism using statistical physics models. To interpret the IBP adsorption mechanism at molecular level, three advanced statistical physics models were employed. Modeling results indicated that IBP adsorption on Zeo-Sep and O-Sep was associated to the formation of two layers. It has been deduced that the IBP adsorption occurred by horizontal and non-horizontal orientations on both adsorbents depending on the temperature thus reflecting that the adsorption was a multi-docking and multi-molecular process, respectively. At high temperature (i.e., 60 °C), it was found that the number of captured IBP molecules is around two reflecting that the IBP was aggregated (i.e., formation of a dimer) in solution. IBP adsorption capacity at saturation was higher on O-Sep than that of Zeo-Sep at all tested temperatures indicating that the O-Sep adsorbent was more suitable for the removal of this pharmaceutical. The interactions between IBP and both adsorbents (IBP/O-Sep, and IBP/Zeo-Sep) and between IBP molecules (IBP- IBP) have been calculated to further characterize the adsorption mechanism, which was found to be a physisorption process. These new findings provided microscopic explanations regarding the IBP adsorption mechanism using clay-based adsorbents.

Keywords: Ibuprofen, organo-sepiolite, zeolite/sepiolite heterostructure, double layer model.

1. Introduction

The removal of pharmaceutical compounds from environment has become a major research subject. The large application of pharmaceuticals regarding the treatment of diseases of humans and animals includes the use of non-steroidal anti-inflammatory drugs due to their analgesic, anti-inflammatory and antipyretic characteristics [1]. Studies have demonstrated that the presence of pharmaceutical compounds in wastewaters can cause serious environmental problems and, consequently, they are considered as toxic pollutants [2-4]. Ibuprofen (IBP) is among the most detected pharmaceuticals in water due to its widespread use [5]. Specifically, recent researches have indicated that the IBP can be found in surface waters at concentrations up to $\mu\text{g/L}$ [6,7]. Different techniques have been applied to reduce the concentration of IBP from water such as biodegradation [8], ultrasonic irradiation [9], chlorination [10], ozonation [11], photocatalysis [41, 42] and adsorption [12]. Due to its easy operation and low cost, the adsorption process is a promising treatment technique for IBP removal from water [13-15]. According to literature, a variety of adsorbents has been synthesized and used to study the IBP removal, mostly activated carbons [16,17], but also mesoporous silicas [18] or metal organic frameworks among others. IBP adsorption using activated carbon is of great interest because this adsorbent is usually characterized by a specific surface chemistry and high surface area [19,20]. However, the utilization of commercial activated carbons could increase the operational costs of IBP removal because only a low percentage of these adsorbents (i.e., usually $< 40\%$) can be regenerated and reused after the adsorption process [21,22]. In the last years, clay materials have attracted a significant attention for various reasons as their swelling properties and high cation exchange capacity [23-25]. Herein, two new materials, namely zeolite/sepiolite nanoheterostructure (Zeo-Sep) and a modified organo-sepiolite (O-Sep), have been synthesized and employed as derived-clay adsorbents to analyze the removal mechanism of IBP from water. Note that the

correlation between experimental and theoretical results can be the key for a better explanation of the mechanism involved in the adsorption of pharmaceuticals. The adsorption isotherms of IBP on Zeo-Sep and O-Sep have been quantified at different temperatures and these experimental data have been used to model and study the IBP adsorption. Several studies demonstrated that the IBP adsorption can imply a monolayer or a multilayer process. Hence, the objective of this paper was to experimentally and theoretically study the IBP adsorption mechanism. In particular, statistical physics models were used to analyze the IBP adsorption. These models assumed that the adsorption of IBP on both adsorbents was performed with the formation of a constant (one or two layers) or a variable number of layers. The estimation of the formed number of layers during the IBP adsorption can play a relevant role for a better description of IBP adsorption mechanism. Contrary to the classical adsorption models such as Langmuir equation that assumes that each active site of any investigated adsorbent captures only one IBP molecule, all the applied statistical physics models assumed that the binding sites of adsorbents can accept a variable number of molecules of this pharmaceutical. These models were useful to obtain new interpretations at molecular level including an energetic study and led to a deeper analysis of the IBP adsorption mechanism on tested clay-based materials.

2. Experimental section

2.1. Materials

The commercial organo-sepiolite (O-Sep) was supplied by TOLSA company. O-Sep is a raw sepiolite modified with organic cations, such as Tetranyl[®] B-2MTH (stearyl dimethyl bencyl ammonium chloride) that was prepared from the commercial tensioactive cations stearalkonium chloride using 32.4 mmol of organo-cation per 100 g of compound. Zeolite/sepiolite nanoheterostructure (Zeo-Sep) was synthesized according to the method described by Gómez-Avilés et al. [26] using a rheological grade sepiolite (named PANGEL

S9) supplied by TOLSA company. Tetraethoxysilane (TEOS, $\geq 99.0\%$ Aldrich), tetrapropylammonium hydroxide (TPAOH) with a 1.0 M concentration in aqueous solution (Sigma-Aldrich) and pellets of NaOH (pure Panreac) were used as reactants for the Zeo-Sep preparation. Ibuprofen (purity $> 99\%$, Sigma Aldrich) was selected as target compound for performing the adsorption studies. Acetonitrile (HPLC grade) and acetic acid (purity $\geq 99\%$) purchased from Scharlau and Sigma Aldrich, respectively, were used as mobile phase for liquid chromatography. Ultrapure water (Type I, $18.2 \text{ M}\Omega\cdot\text{cm}$) and deionized water (Type II) were utilized in this work.

2.2 Liquid-phase adsorption experiments

The adsorption experiments were performed by adding an adsorbent load of $250 \text{ mg}\cdot\text{L}^{-1}$ to ibuprofen solutions with different initial concentrations. The suspensions were stirred at 170 rpm for 24 h at different temperatures in a water bath orbital shaker. Samples of 1 mL were collected at different times and filtered using PTFE syringe filters (Whatman $0.45 \text{ }\mu\text{m}$). The adsorption isotherms were carried out at three different temperatures (20, 40 and $60 \text{ }^{\circ}\text{C}$) using the same adsorbent load and varying the concentration of ibuprofen from 5 to $80 \text{ mg}\cdot\text{L}^{-1}$. Since IBP has a limited solubility at room temperature, these solutions were prepared at $60 \text{ }^{\circ}\text{C}$ obtaining supersaturated solutions. The resulting pH varied from 6.2 to 7.3 for the IBP solutions at 80 and $5 \text{ mg}\cdot\text{L}^{-1}$, respectively. The concentration of ibuprofen in the liquid phase was determined by HPLC using a Shimadzu Prominence-I LC-2030C chromatograph equipped with a diode array detector (SPD-M30A) and a C18 column (Eclipse Plus $5 \text{ }\mu\text{m}$, Agilent). The mobile phase was a mixture of acetonitrile-acetic acid (0.1 v/v% in type I water) using an isocratic method (50:50%) with a flow rate of $0.9 \text{ mL}\cdot\text{min}^{-1}$. The wavelength was set to 222 nm for the detection of IBP that appeared at 10 min retention time. A material balance was utilized to calculate the corresponding adsorption capacities of IBP.

2.3 Characterization techniques

X-ray diffraction (XRD) patterns of the clay-based adsorbents were recorded on a Bruker D8 diffractometer working at 40 kV and 30 mA with Ni-filtered Cu K α radiation. Textural parameters of these adsorbents were determined via N₂ adsorption-desorption, which were obtained at -196 °C using a Micromeritics TriStar II apparatus. Samples (150-200 mg) were previously outgassed at 120 °C overnight. BET surface area (S_{BET}) was calculated by the Brunauer-Emmett-Teller (BET) method [41]. The external (or non-microporous area S_{EXT}) and the micropore volume (V_t) were obtained from the t-plot by De Boer's method [27]. The total pore volume (V_p) of the adsorbents was estimated from the amount of nitrogen adsorbed (expressed as liquid) at a relative pressure of 0.99. The micropore size distribution was assessed by the density functional theory (DFT) [28]. Scanning electron microscopy (SEM) images were obtained with a Quanta 3D FEG apparatus from FEI Company. A Tecnai G220 microscope (FEI COMPANY) working at 200 kV accelerating voltage was used to obtain the transmission electron microscopy (TEM) images. Fourier Transform Infrared (FTIR) spectra were recorded on a Bruker IFS 66V-S spectrometer (Bruker, Billerica, MA, USA) using a resolution of 2 cm⁻¹ in the range 4000–400 cm⁻¹. Samples were previously prepared using KBr pellets (2 wt% sample concentration and pelletized at 10 Ton). The pH at the point of zero charge (pH_{pzc}) was determined using the pH drift method [43]. For that purpose, 50 mL of NaCl solution 0.01 M were placed in a closed titration vessel. The pH was adjusted from 3 to 11 using 0.1 M HCl or NaOH. Further, 20 mg of each adsorbent were suspended and nitrogen was bubbled during 30 min in order to stabilize the initial pH by removing dissolved gasses. After 5 h, the final pH was measured and plotted versus the initial one where the pH value in which the $\text{pH}_{\text{initial}} = \text{pH}_{\text{final}}$ corresponds to the pH_{pzc} .

3. Description of IBP adsorption isotherm profiles and model expressions

Figures 1a and 1b show the IBP adsorption isotherms at 20, 40 and 60 °C on O-Sep and Zeo-Sep adsorbents, respectively. IBP adsorption equilibrium capacities tend to a constant value at high concentration reflecting the typical saturation phenomenon in a liquid-phase adsorption. This phenomenon is the result of the pore filling of both adsorbents with IBP molecules by the formation of one or more adsorbed layers. Based on the IBP isotherm profiles, three advanced statistical physics models were selected to mathematically discuss and analyze the pharmaceutical adsorption mechanism.

3.1 Model 1: Adsorption with the formation of one layer

This model defined that the IBP adsorption occurred by a constant number of layer (1 layer in this case), but assuming that the adsorption sites of Zeo-Sep and O-Sep captured a variable number of pharmaceutical molecules contrary to the fundamentals of the Langmuir model. This variable was defined as the number of captured IBP molecules per adsorbent site parameter. In terms of the energy involved in the adsorption process, the first model supposed that the IBP adsorption on both adsorbents was associated to a constant energy (ϵ). The expression of the model is given by the following expression [29,30]:

$$Q_e = \frac{nD_m}{1 + \left(\frac{C_{1/2}}{C}\right)^n} \quad (1)$$

where n is defined as the captured number of IBP molecule per Zeo-Sep and O-Sep site, D_m is the density of receptor sites of these adsorbents and $C_{1/2}$ (mg/L) is the concentration at half-saturation of the formed layer.

3.2 Model 2: adsorption with the formation of a double layer

This model also established that the IBP adsorption on the adsorbents was performed with a constant number of layers, although in this case 2 layers are assumed. The main active sites

for the IBP adsorption can capture a variable number of the pharmaceutical molecules. Two energies are considered regarding the second model that are related to IBP- Zeo-Sep and O-Sep, and IBP-IBP interactions. The expression of second model is given by [31]:

$$Q_e = nD_m \frac{\left(\frac{C}{C_1}\right)^n + 2\left(\frac{C}{C_2}\right)^{2n}}{1 + \left(\frac{C}{C_1}\right)^n + \left(\frac{C}{C_2}\right)^{2n}} \quad (2)$$

where C_1 and C_2 are defined as two concentrations at half-saturation that are related to the first and second formed layers, while D_m is the density of receptor sites. The expression of both adsorption energies are given by

$$\Delta E_1 = R \cdot T \cdot \ln(C_s/C_1) \quad (3)$$

$$\Delta E_2 = R \cdot T \cdot \ln(C_s/C_2) \quad (4)$$

where C_s (mg/L) is the IBP water solubility.

Note that the first step to calculate the model expression corresponded to the expression of the partition function that is related to one active site. So, the expression for one site is given by:

$$Z_{gc} = 1 + e^{\beta(\varepsilon_1 + \mu)} + e^{\beta(\varepsilon_1 + \varepsilon_2 + 2\mu)} \quad (5)$$

while the total expression of the partition function for D_m receptor sites is given by:

$$Z_{gc} = (Z_{gc})_{m}^D \quad (6)$$

3.3 Model 3: adsorption with a variable number of layers

This third model assumed that the IBP adsorption was achieved by a variable number of layers (N_2+1), and each adsorption site captures also a variable number of IBP molecules. Two energies are analyzed to characterize the adsorption: the first energy describes the

interactions between IBP and adsorbent surface and it is mainly related to the first layer (IBP-Zeo-Sep and O-Sep), and the second energy is related to the interactions between IBP molecules (IBP-IBP) (where N_2 is variable). Consequently, the total variable number of layers is $1+N_2$ and the expression of the third model is given by the equation [31]:

$$Q_e = nD_m \frac{\frac{-2\left(\frac{C}{C_1}\right)^{2n}}{1-\left(\frac{C}{C_1}\right)^n} + \frac{\left(\frac{C}{C_1}\right)^n \left(1-\left(\frac{C}{C_1}\right)^{2n}\right)}{\left(1-\left(\frac{C}{C_1}\right)^n\right)^2} + \frac{2\left(\frac{C}{C_1}\right)^n \left(\frac{C}{C_2}\right)^n \left(1-\left(\frac{C}{C_2}\right)^{nN_2}\right)}{\left(1-\left(\frac{C}{C_2}\right)^n\right)} + \frac{N_2 \left(\frac{C}{C_1}\right)^n \left(\frac{C}{C_2}\right)^n \left(\frac{C}{C_2}\right)^{nN_2}}{\left(1-\left(\frac{C}{C_2}\right)^n\right)} + \frac{\left(\frac{C}{C_1}\right)^n \left(\frac{C}{C_2}\right)^{2n} \left(1-\left(\frac{C}{C_2}\right)^{nN_2}\right)}{\left(1-\left(\frac{C}{C_2}\right)^n\right)^2}}{\frac{\left(1-\left(\frac{C}{C_1}\right)^{2n}\right)}{\left(1-\left(\frac{C}{C_1}\right)^n\right)} + \frac{\left(\frac{C}{C_1}\right)^n \left(\frac{C}{C_2}\right)^n \left(1-\left(\frac{C}{C_2}\right)^{nN_2}\right)}{\left(1-\left(\frac{C}{C_2}\right)^n\right)}} \quad (7)$$

where C_1 and C_2 are the concentrations at half-saturation of the first and the other N_2 formed layer, respectively.

These statistical physics adsorption models were fitted to the adsorption isotherms at different temperatures in order to estimate the probable number of layers formed during the adsorption process. Results of this data correlation were utilized to select the proper adsorption model for performing the theoretical analysis. The mathematical fitting was based on Levenberg-Marquardt algorithm using a multivariable non-linear regression [31]. All values of the determination coefficient R^2 of both adsorption systems varied from 0.961 to 0.974, 0.977 to 0.991 and 0.978 to 0.994 for the first, second and third models, respectively. Based on these results, the first model was discarded because its low values of R^2 that indicated that it was not able to accurately describe the IBP adsorption mechanism. Regarding the models 2 and 3, it is clear that the difference between the R^2 values is not significant and they are relatively

close to unity. Note that it was mentioned in Section 3 that the models 2 and 3 defined that the IBP adsorption can occur by the formation of two and a variable number of layers, respectively. The total number of formed layers regarding the model 3 can be equal, inferior or superior to 2. Results of isotherms fitting demonstrated that the total number of formed layers ($1+N_2$) assumed by the third model varies from 1.87 and 2.12. Therefore, this information indicated that the adsorption of IBP on both adsorbents was performed by a constant number of layers, which is equal to 2. Consequently, the model 2 was selected to interpret the IBP adsorption mechanism. All estimated values of parameters of model 2 are listed in Table 1.

4. Results and discussion

4.1 Physicochemical characterization

The adsorbents were characterized by XRD in order to analyze their structural properties. Figure 2 shows the XRD pattern of the O-Sep that presents the characteristic peaks of the raw sepiolite (JCPDS data No. 130595), with the main (110) reflection at 1.20 nm. Although O-Sep is an organoclay modified with tensioactive compounds, their presence does not modify the sepiolite structure because its fibrous morphology. The XRD pattern of Zeo-Sep heterostructure is also shown in Figure 2. As stated, this adsorbent has been prepared following a reported methodology based on the zeolite growth over a sepiolite [26]. The diffraction peaks correspond to the characteristic reflections of calcined zeolite MFI [32], and their presence corroborates the successful preparation of the desired material. Zeo-Sep sample does not show the characteristic (110) reflection of the sepiolite because a thermal treatment at 600 °C is required to obtain the final heterostructure and, in these conditions, the sepiolite structure changes to enstatite, whose reflections peaks overlapped with those of zeolite.

Since the adsorption properties of different materials depends on their textural properties, the N₂ adsorption-desorption isotherms at – 196 °C has been carried out (Figure 3). O-Sep sample displays an isotherm of type II, according to IUPAC classification [33], with a closed hysteresis loop that could be classed as type II according to the sub-classification introduced by Rouquerol et al. [33]. This kind of isotherms is characteristic of mesoporous materials. By the other side, Zeo-Sep adsorbent shows a very different isotherm that can be classified as type IV according to IUPAC [33]. This class of isotherms is associated to mesoporous materials with a significant contribution of microporosity, as indicates the relatively high amount of N₂ adsorbed at low relative pressures. In this case, it can be observed a step close to $P/P_0 = 0.2$ typical of N₂ adsorption in high-silica MFI, which is due to a phase transition in the adsorbate phase (Figure 3) [34]. The textural parameters of both materials obtained from N₂ isotherms are collected in Table 2. O-Sep has a relatively low surface area ($64 \text{ m}^2\cdot\text{g}^{-1}$) and does not exhibit microporosity mainly due to the presence of the surfactant at sepiolite surface. Zeo-Sep has a high surface area ($300 \text{ m}^2\cdot\text{g}^{-1}$) with a high contribution of microporosity (about 65%) mainly due to the formation of a crystalline MFI zeolite. These results evidence the textural differences among both selected adsorbents. The morphology of the materials was studied by SEM and TEM microscopies. O-Sep adsorbent (Figure 4A) displays big aggregates of sepiolite fibres that form a heterogeneous and irregular morphology. On the other side, Zeo-Sep (Fig. 4B) depicts particles of $\approx 5 \text{ }\mu\text{m}$ that are constituted by a heterogeneous distribution of zeolite particles and fibrous sepiolite. This morphology is more evident in TEM image as shown in Figure 4d. Zeolite particles have a like-sphere morphology, with a size close to $0.1 \text{ }\mu\text{m}$, that are anchored at sepiolite fiber surface. This interesting morphology yields a material with high surface area.

Figure 5 shows the FTIR spectra of both adsorbents used in IBP removal. O-Sep displays the characteristic bands of a sepiolite with organic moieties (surfactant) at surface. Thus, the

stretching $\nu_{\text{C-H}}$ vibration bands associated to the alkylammonium chains ions appear at 2928 and 2855 cm^{-1} , while the bending δ_{HCH} vibration is located at 1464 cm^{-1} . The stretching $\nu_{\text{O-H}}$ vibrations appears in the 3700-3200 cm^{-1} region associated with the adsorbed water molecules and different hydroxylated groups, being the band at 3686 cm^{-1} related with the $\nu_{\text{O-H}}$ of the Mg-OH group. Although sepiolite materials usually show a characteristic band at 3720 cm^{-1} due to Si-OH bonds, O-Sep does not display this band because the presence of alkylammonium molecules at surface that blockage the silanol groups [35]. The presence of water adsorbed at surface is also evident because the bending δ_{HOH} bands that appear in the 1700-1600 cm^{-1} region. The other bands observed between 1200 and 400 cm^{-1} correspond to Mg-O stretching vibrations in the octahedral sheet and to Si-O bonds in the tetrahedral sheet of the sepiolite [36]. These results corroborate the presence of both organic and hydroxyl species at surface of O-Sep. FTIR spectrum of the Zeo-Sep (Figure 5) just shows the characteristic peaks of the zeolite and the vibrations related with water adsorbed at surface ($\nu_{\text{O-H}}$ at 3434 and δ_{HOH} at 1633). The bands at 1229 and 1111 cm^{-1} are associated, respectively, to internal and external asymmetric stretching $\nu_{\text{Si-O}}$ vibrations of SiO_4 , and the respective symmetric vibration appears at 801 cm^{-1} [37]. At lower wavenumbers, the bands assigned to bending vibrations, $\delta_{\text{O-Si-O}}$ and $\delta_{\text{Si-O-Si}}$ appear at 555 and 455 cm^{-1} , respectively, which corroborates the formation of the characteristic Si-O bonds of zeolite crystals. Unlike, the O-Sep, Zeo-Sep has only water adsorbed at the surface.

An important parameter regarding the adsorption behaviour of the adsorbents is the pH_{pzc} . The resulting values were 9.2 and 8.3 for Zeo-Sep and O-Sep, respectively. It is noteworthy that the presence of zeolite crystals at Zeo-Sep yields an adsorbent with a fairly higher pH_{pzc} , probably due to the presence of basic groups from the zeolite. The adsorption capacity of an adsorbent depends on multiple interactions, being the electrostatic forces one of them. Since the IBP adsorption was performed at initial pH from 6.2-7.3, depending on the IBP initial

concentration, and the pK_a of IBP is 4.9, the molecules of the IBP are negatively charged. In contrast, the pH_{pzc} of both adsorbents is above the adsorption pH, resulting in a surface partially positively charged. Therefore, the IBP adsorption is favoured in both adsorbents by attractive electrostatic forces between the negatively charged IBP molecules and the positive character of the solid surface.

4.2 Explanation of IBP adsorption mechanism via the statistical physics parameters n , D_m , and Q_{sat}

The parameter n included in the model 2 can provide steric explanations regarding the IBP adsorption mechanism on both adsorbents. This parameter is also capable to estimate the aggregation degree of IBP [31]. In other direction, this parameter can simply attribute a clear idea about the orientation of IBP on Zeo-Sep and O-Sep by the analysis of its values obtained from isotherms fitting [31]. Note that the Langmuir model is among the most common models applied to study the adsorption of pharmaceuticals on different adsorbents defining that each binding site of any tested adsorbent accepts one molecule [39, 42]. This general assumption proved that the orientation of pharmaceutical molecules is inclined on the adsorbent surface. This is not always correct because there are many factors mainly related to the adsorbate structure, adsorbent properties or external experimental operating parameters that can lead to a change of binding orientation during the adsorption process. Results of Table 2 clearly indicate that the parameter n varies as a function of adsorption temperature. At low temperature (e.g., 20 and 40 °C), the values of this parameter are 0.44 and 0.52 for IBP-Zeo-Sep, and 0.53 and 0.88 for IBP-O-Sep, but at high temperature the values of parameter n are around to 2.00 (i.e., 1.95 for IBP- Zeo-Sep and 2.10 for O-Sep, respectively). At 20 and 40 °C, it was suggested that the main active site of Zeo-Sep and O-Sep captured a fraction of IBP molecule generating an interaction with more than one active site. This fact suggested a

parallel orientation of IBP on both adsorbents implying a multi-docking process. Contrary to this behavior, it is clear that the responsible binding site for the adsorption captured around two IBP molecules implying a multi-molecular adsorption process with an inclined orientation on Zeo-Sep and O-Sep at 60 °C. The change of IBP adsorption orientation from a parallel to an inclined position as a function of temperature is probably due to the thermal collisions between IBP molecules. Indeed, the thermal collisions of pharmaceutical molecules increase with temperature and it can cause a change regarding the IBP orientation on both adsorbents. In another direction, the ibuprofen formed an aggregate in solution (before adsorption) at high temperature (i.e., 60 °C) mainly as a dimer since the parameter values of n are around 2. The aggregation of IBP can be explained by the increment of temperature that generated an activation energy that facilitates the bindings between IBP molecules. Comparatively, the number of captured pharmaceutical molecules by the adsorbent active site varies as follows: $n(\text{IBP-O-Sep}) > n(\text{IBP-Zeo-Sep})$ at all tested temperatures. Chemically speaking, this sequence can be explained by the affinity of the adsorbent. Moreover, when an adsorbent contains a significant amount of functional groups, the capture of pharmaceutical molecules is easier. If the textural properties of adsorbent are analyzed, it is clear that the difference in the capture of pharmaceutical molecules is probably due to the difference of porosity. Note that the total pore volumes are quite similar, but the Zeo-Sep has a higher contribution of microporosity.

Figure 6 explained the effect of temperature on the parameter D_m , which is the density of receptor sites. The reduction of this parameter as a function of adsorption temperature is reasonable explained by the increment of the number of captured IBP per active site of both adsorbents. Indeed, the increment of the number of IBP on the active site can limit the space on both adsorbents. A significant reduction of D_m at high temperature (60 °C) was observed.

This is due to the aggregation phenomenon that hides the most accessible binding sites for the IBP adsorption.

The correlation of these parameters (n and D_m) and the constant number of layers can be observed via the adsorption capacity and its variation with the temperature, which is depicted in Figure 7. According to the model 2, the expression of the adsorption capacity at saturation is: $Q_{sat} = 2 \cdot n \cdot D_m$. Note that the expression for Q_{sat} has been obtained by applying the limit when the equilibrium concentration of IBP tends to infinity in the adsorption model. As stated in this section, the increment of temperature led to an increment of the parameter n and to a decrement of the parameter D_m . Since the number of formed layers during the IBP adsorption is constant, the variation of this parameter is mainly related to the variation of n and D_m . Based on these findings, it can be concluded that the reduction of the parameter Q_{sat} as a function of temperature is due to the decrement of D_m parameter generating an exothermic adsorption process. In terms of the performance of IBP-O-Sep and IBP-Zeo-Sep, it was concluded that: $Q_{sat} \text{ (IBP-O-Sep)} > Q_{sat} \text{ (BP-Zeo-Sep)}$. This trend suggested that the adsorbent O-Sep is more effective to adsorb the IBP, despite its significantly lower total surface area, and this difference is probably due to the higher adsorbent affinity.

4.3 Characterization of the IBP adsorption mechanism via the adsorption energy

The model 2 provided two adsorption energies ΔE_1 and ΔE_2 (see expressions 3 and 4) depending on the concentration at half-saturation (C_1 and C_2) of the first and second adsorbed layers, respectively, and the solubility (C_s) of IBP in water, which are related to the interactions between IBP and adsorbents and the self-interactions of IBP molecules. All the estimated mean energies are lower than 25 kJ/mol reflecting that the IBP adsorption is a physisorption process and they are also negative corroborating that this removal process is exothermic. As a first conclusion, the parameter D_m contributes in the decrement of the adsorption capacity at saturation for both adsorbents. Referring to literature, some studies

have indicated that the adsorption capacity for the removal of pharmaceuticals depended on the adsorbent surface area [38, 39]. Table 2 shows that the BET surface of O-Sep ($83 \text{ m}^2/\text{g}^{-1}$) is inferior than that of Zeo-Sep ($307 \text{ m}^2/\text{g}^{-1}$). However, there is no a trend with the variation of adsorption capacity where Q_{sat} (IBP-O-Sep) $>$ Q_{sat} (IBP-Zeo-Sep). This fact clearly indicates that the BET surface of both adsorbents is not the main factor to justify the variation of these adsorption capacities. On the other hand, it was concluded that ΔE_1 (IBP-O-Sep) $>$ ΔE_1 (IBP-Zeo-Sep), and ΔE_2 (IBP-O-Sep) $>$ ΔE_2 (IBP-Zeo-Sep), which followed the variation of IBP adsorption capacities. This evidence reflected that the adsorption energy is also a second parameter that contributes to control the IBP adsorption mechanism. In summary, the IBP adsorption mechanism was expected to be controlled by the density of receptor sites and both adsorption energies.

Conclusions

The adsorption mechanism of IBP on adsorbents O-Sep and on Zeo-Sep was experimentally and theoretically studied. Experimental results indicated that the adsorption of IBP on both adsorbents tended to a saturation phenomenon resulting a formation of one or more layers. Based on the modeling analysis, it was demonstrated that the IBP adsorption mechanism was associated to the formation of two adsorbed layers. A statistical physics model showed that the parallel and non-parallel adsorption orientations of the IBP on both adsorbents are possible depending on the temperature. At high temperature, the model demonstrated that the IBP molecules aggregated in solution and mainly formed a dimer. It was also noted that the density of receptor sites and the adsorption energies are the main factors explaining the IBP adsorption mechanism. The theoretical study of the adsorption energy corroborated that the IBP adsorption process is exothermic.

References

- [1] J.A. Muthanna. Adsorption of non-steroidal anti-inflammatory drugs from aqueous solution using activated carbons: Review. *J. Environ. Manage.* 190 (2017) 274–282.
- [2] J. Wilkinson, P.S. Hooda, J. Barker, S. Barton, J. Swinden. Occurrence, fate and transformation of emerging contaminants in water: an overarching review of the field. *Environ. Pollut.* 231 (2017) 954–970.
- [3] R.R.Z. Tarpani, A. Azapagic. Life cycle environmental impacts of advanced wastewater treatment techniques for removal of pharmaceuticals and personal care products (PPCPs). *J. Environ. Manag.* 215 (2018) 258–272.
- [4] N.H. Tran, M. Reinhard, K.Y.H. Gin. Occurrence and fate of emerging contaminants in municipal wastewater treatment plants from different geographical regions-a review. *Water Res.* 133 (2018) 182–207.
- [5] P. Verlicchi, A. Galletti, M. Petrovic, D. Barcelo. Hospital effluents as a source of emerging pollutants: an overview of micropollutants and sustainable treatment options. *J Hydrol.* 389 (2010) 416–28.
- [6] T. Deblonde, C. Cossu-Leguille, P. Hartemann. Emerging pollutants in wastewater, a review of the literature. *Int. J. Hyg Environ. Health* 214 (2011) 442–448.
- [7] Z. Hasan, N.A. Khan, S.H. Jhung. Adsorptive removal of diclofenac sodium from water with Zr-based metal-organic frameworks. *Chem. Eng. J.* 284 (2016) 1406–1413.
- [8] A. Joss, S. Zabczynski, A. Göbel, B. Hoffmann, D. Löffler, C.S. McArdell, T.A. Ternes, A. Thomsen, H. Siegrist. Biological degradation of pharmaceuticals in municipal wastewater treatment: proposing a classification scheme. *Water Res.* 40 (2006) 1686–1696

- [9] F. Méndez-Arriaga, R.A. Torres-Palma, C. Petrier, S. Esplugas, J. Gimenez, C. Pulgarin. Ultrasonic treatment of water contaminated with ibuprofen. *Water Res.* 42 (2008) 4243–8.
- [10] G.R. Boyd, S. Zhang, D.A. Grim. Naproxen removal from water by chlorination and biofilm processes. *Water Res.* 39 (2005) 668–676
- [11] S. Esplugas, D.M. Bila, L. Gustavo, T. Krause, M. Dezotti. Ozonation and advanced oxidation technologies to remove endocrine disrupting chemicals (EDCs) and pharmaceuticals and personal care products (PPCPs) in water effluents. *J. Hazard Mater.* 149 (2007) 631–664.
- [12] I.A. Katsoyiannis, S. Canonica, U. von Gunten. Efficiency and energy requirements for the transformation of organic micropollutants by ozone, O_3/H_2O_2 and UV/H_2O_2 . *Water Res.* 45 (2011) 3811–3822.
- [13] Z.Q. Cai, A.D. Dwivedi, W.N. Lee, X. Zhao, W. Liu, M. Sillanpaa, D.Y. Zhao, C.H. Huang, J. Fu. Application of nanotechnologies for removing pharmaceutically active compounds from water: development and future trends. *Environ. Sci. Nano* 5 (2018) 27–47.
- [14] Z.J. Li, Z.W. Huang, W.L. Guo, L. Wang, L.R. Zheng, Z.F. Chai, W.Q. Shi. Enhanced photocatalytic removal of uranium(VI) from aqueous solution by magnetic TiO_2/Fe_3O_4 and its graphene composite. *Environ. Sci. Technol.* 51 (2017) 5666–5674.
- [15] W.Q. Shi, L.Y. Yuan, C.Z. Wang, L. Wang, L. Mei, C.L. Xiao, L. Zhang, Z.J. Li, Y.L. Zhao, Z.F. Chai. Exploring actinide materials through synchrotron radiation techniques. *Adv. Mater.* 26 (2014) 7807–7848.
- [16] A.S. Mestre, J. Pires, J.M.F. Nogueira, J.B. Parra, A.P. Carvalho, C.O. Ania. Waste derived activated carbons for removal of ibuprofen from solution: role of surface chemistry and pore structure. *Bioresource Technol.* 100 (2009) 1720–6.

- [17] A.S. Mestre, J. Pires, J.M.F. Nogueira, A.P. Carvalho. Activated carbons for the adsorption of ibuprofen. *Carbon* 45 (2007) 1979–88.
- [18] Y.F. Zhu, J.L. Shi, Y.S. Li, H.R. Chen, W.H. Shen, X.P. Dong. Storage and release of ibuprofen drug molecules in hollow mesoporous silica spheres with modified pore surface. *Micropor. Mesopor. Mater.* 85 (2005) 75–81.
- [19] L. Li, P.A. Quinlivan, D.R.U. Knappe. Effects of activated carbon surface chemistry and pore structure on the adsorption of organic contaminants from aqueous solution. *Carbon* 40 (2003) 2085–2100.
- [20] A. Dabrowski, P. Podkoscielny, Z. Hubicki, M. Barczak. Adsorption of phenolic compounds by activated carbon – a critical review. *Chemosphere* 58 (2005) 1049–1070.
- [21] L. Wang, N. Balasubramanian. Electrochemical regeneration of granular activated carbon saturated with organic compounds. *Chem. Eng. J.* 155 (2009) 763–768.
- [22] P.K. Sharma, P.C. Wankat. Solvent recovery by steamless temperature swing carbon adsorption processes. *Ind. Eng. Chem. Res.* 49 (2010) 11602–11613.
- [23] G. Lagally. Pesticides-clay interactions and formulations. *Appl. Clay Sci.* 18 (2001) 205–209.
- [24] M.D. Alba, M.A. Castro, M. Naranjo, E. Pavón. Hydrothermal reactivity of Na-nMicas ($n = 2, 3, 4$). *Chem. Mater.* 18 (2006) 2867–2872.
- [25] D. Zadaka, Y.G. Mishael, T. Polubesova, C. Serban, S. Nir. Modified silicates and porous glass as adsorbents for removal of organic pollutants from water and comparison with activated carbon. *Appl. Clay Sci.* 36 (2007) 174–181.

- [26] A. Gómez Avilés, C. Belver, P. Aranda, E. Ruiz-Hitzky, M.A. Camblor. Zeolite-sepiolite nanoheterostructures. *J. Nanostruct. Chem.* 4 (2014) 90.
- [27] B.C. Lippens, J.H. De Boer. Studies on pore systems in catalysts: V. The t method. *J. Catal.* 4 (1965) 319–323.
- [28] J. Landers, G.Y. Gor, A.V. Neimark. Density functional theory methods for characterization of porous materials. *Colloids Surf. A: Physicochem. Eng. Asp.* 437 (2013) 3–32.
- [29] L. Sellaoui, G.L. Dotto, A. Ben Lamine, A. Erto. Interpretation of single and competitive adsorption of cadmium and zinc on activated carbon using monolayer and exclusive extended monolayer models. *Environ. Sci. Pollut. Res.* 24 (2017) 19902–19908.
- [30] L. Sellaoui, F.E. Soetaredjo, S. Ismadji, C.E. Lima, A. Ben Lamine, A. Erto. New insights into single-compound and binary adsorption of copper and lead ions on treated sea mango shell: Experimental and theoretical studies. *Phys. Chem. Chem. Phys.* 19 (2017) 25927-25937.
- [31] L. Sellaoui, H. Guedidi, S. Knani, L. Reinert, L. Duclaux, A. Ben Lamine. Application of statistical physics formalism to the modeling of adsorption isotherms of ibuprofen on activated carbon. *Fluid Phase Equilibr.* 387 (2015) 103-110.
- [32] C. Baerlocher, L.B. McCusker. Database of Zeolite structures. <http://www.iza-structure.org/databases/> (2018). Accessed 19 April 2019.
- [33] F. Rouquerol, J. Rouquerol, K. Sing. Adsorption by Powders and Porous Solids: Principles, Methodology and Applications. Academic Press, London (1999)

- [34] P.L. Llewellyn, J.P. Coulomb, Y. Grillet, J. Patarin, G. Andre, J. Rouquerol. Adsorption by MFI-type zeolites examined by isothermal microcalorimetry and neutron diffraction. 2. Nitrogen and carbon monoxide. *Langmuir* 9 (1993) 1852–1856.
- [35] J. L. Ahlrichs, C. Y. Serna, J.M. Serratosa. Structural Hydroxyls in Sepiolites. *Clays Clay Miner.* 23 (1975) 119-124.
- [36] T. Y. Perraki, A. Orfanoudaki. Study of Raw and Thermally Treated Sepiolite from the Mantoudi Area, Euboea, Greece X-ray Diffraction, TG/DTG/DTA and FTIR Investigations. *J. Therm. Anal. Calorim.* 91 (2008) 589-593
- [37] E. M. Flanigen. Structural Analysis by IR Spectroscopy" in "Zeolite Chemistry and Catalysis" (Ed.: J. A. Rabo), vol. 171, pp. 80-117, ACS Monograph, American Chemical Society, Washington, 1976.
- [38] Z. Hasan, J. Jeon, S.H. Jhung. Adsorptive removal of naproxen and clofibric acid from water using metal-organic frameworks. *J. Hazard. Mater.* 209–210 (2012) 151–157.
- [39] J. Bedia, C. Belver, S. Ponce, J. Rodriguez, J.J. Rodriguez. Adsorption of antipyrine by activated carbons from FeCl₃-activation of Tara gum. *Chem. Eng. J.* 333 (2018) 58–65.
- [40] M. Akkari, P. Aranda, C. Belver, J. Bedia, A. Ben. Haj. Amarab, E. Ruiz-Hitzky. Reprint of ZnO/sepiolite heterostructured materials for solar photocatalytic degradation of pharmaceuticals in wastewater. *Appl. Clay Sc.* 160 (2018) 3-8.
- [41] S. Brunauer, P.H. Emmett, E. Teller. Adsorption of Gases in Multimolecular Layers. *J. Am. Chem. Soc.* 60 (1938) 309–319.

[42] N. Delgado, D. Capparelli, A. Navarro, D. Marin. Pharmaceutical emerging pollutants removal from water using powdered activated carbon: Study of kinetics and adsorption equilibrium. *J. Environ. Manage.* 236 (2019) 301-308.

[43] G. Newcombe, R. Hayes, M. Drikas. Granular activated carbon: Importance of surface properties in the adsorption of naturally occurring organics. *Colloid Surface A.* 78 (1993) 65–71.

Parameters of model 2						
	T(°C)	<i>n</i>	<i>D_m</i> (<i>mg / g</i>)	<i>Q_{esat}</i> (<i>mg / g</i>)	ΔE ₁ (kJ/mol)	ΔE ₂ (kJ/mol)
IBP- Zeo-Sep	20	0.44	25.19	22.17	-17.22	-13.13
	40	0.52	14.66	15.25	-14.89	-10.88
	60	1.95	4.13	16.14	-12.88	-7.87
IBP- O-Sep	20	0.53	60.61	64.25	-24.18	-17.25
	40	0.88	30.21	53.18	-21.11	-14.14
	60	2.10	11.21	47.11	-15.29	-10.28

Table 1: Estimated values of parameters of model 2 for the adsorption of IBP on Zeo-Sep and O-Sep.

	S_{BET} ($\text{m}^2 \cdot \text{g}^{-1}$) ^a	S_{EXT} ($\text{m}^2 \cdot \text{g}^{-1}$) ^b	S_{MP} ($\text{m}^2 \cdot \text{g}^{-1}$) ^c	V_{MP} ($\text{cm}^3 \cdot \text{g}^{-1}$) ^d	V_{T} ($\text{cm}^3 \cdot \text{g}^{-1}$) ^e
O-Sep	83	83	--	--	0.357
Zeo-Sep	307	102	205	0.095	0.368

^a S_{BET} : specific surface area by BET method; ^b S_{EXT} : external surface, ^c S_{MP} : microporous surface and ^d V_{MP} : micropore volume estimated by t-mehod; ^e V_{T} : total pore volume at $P/P_0=0.99$.

Table 2: Textural parameters of the adsorbents used in IBP removal.

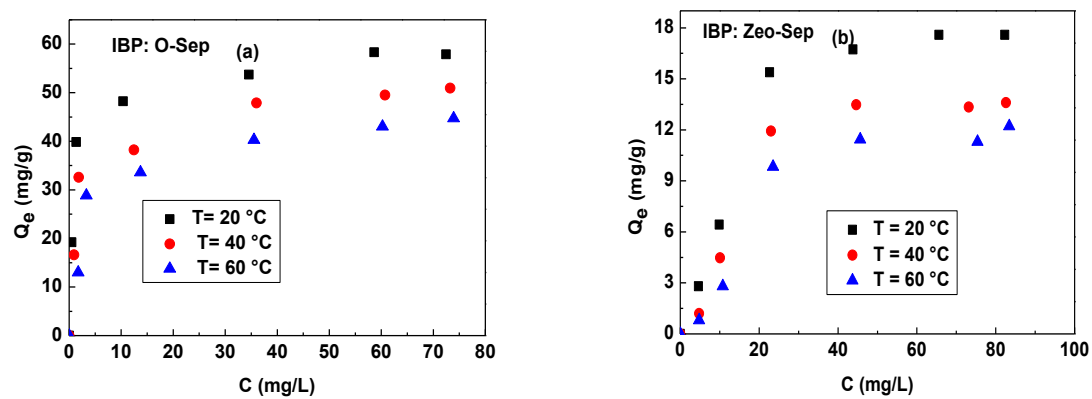


Figure 1: Adsorption isotherms of IBP on **adsorbents** (a) O-Sep, and (b) Zeo-Sep at 20 - 60 °C.

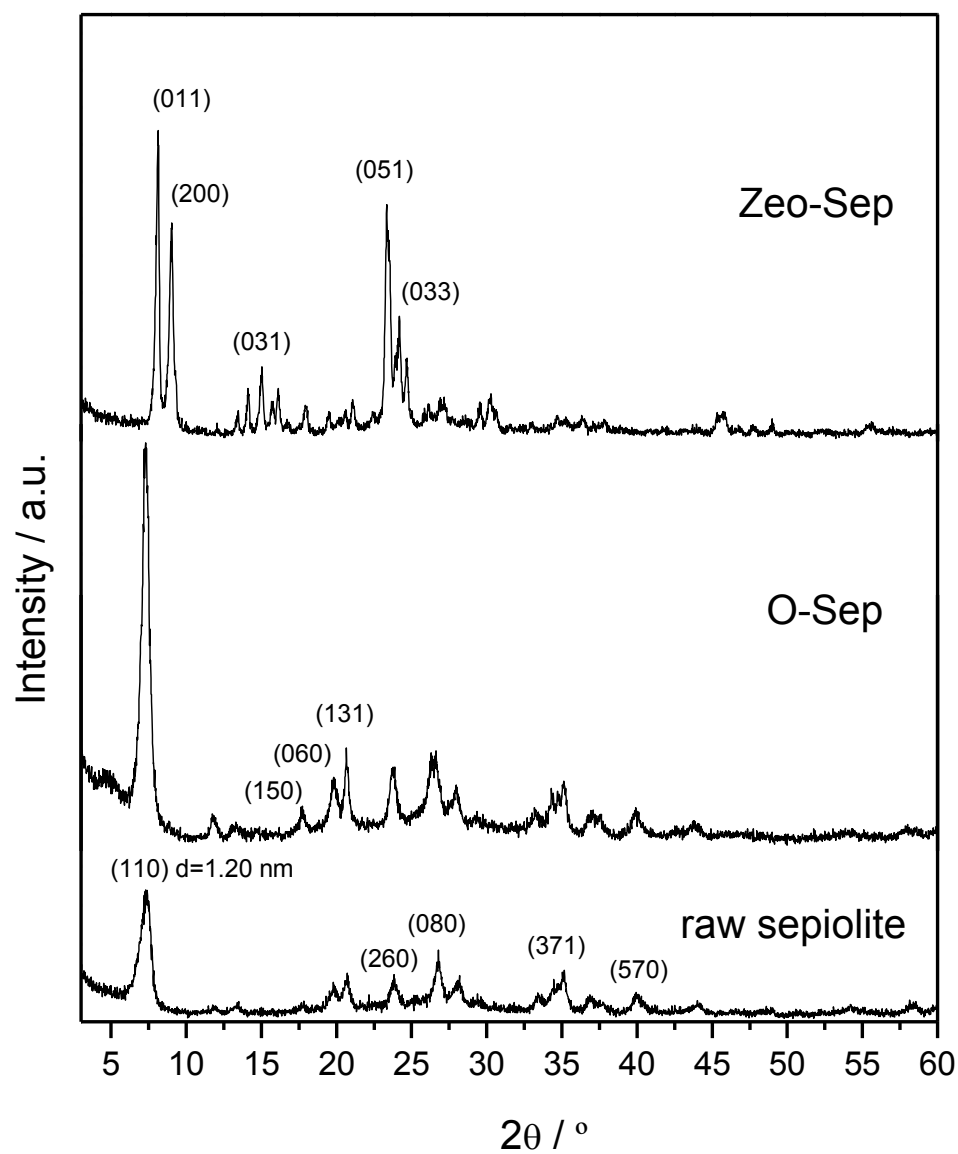


Figure 2: XRD patterns of the commercial O-Sep and the synthesized Zeo-Sep heterostructure compared with the raw sepiolite.

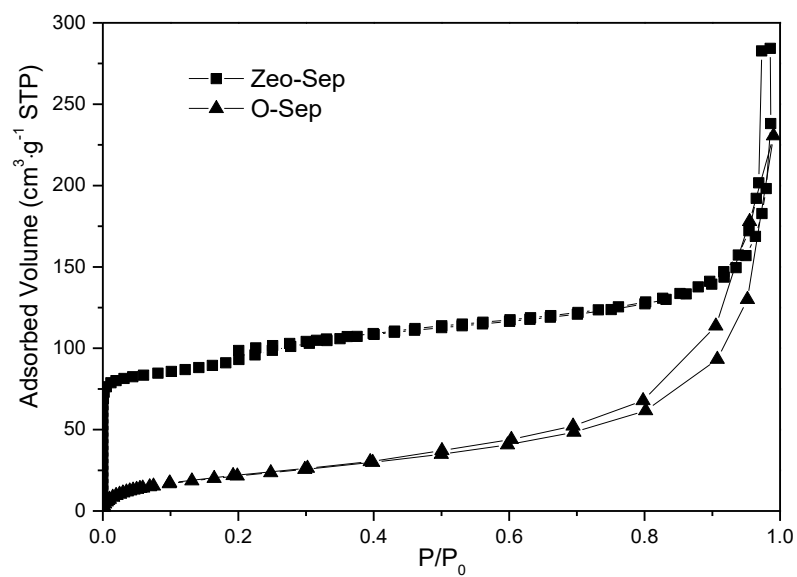


Figure 3: N₂ adsorption-desorption isotherms at -196 °C of O-Sep and Zeo-Sep.

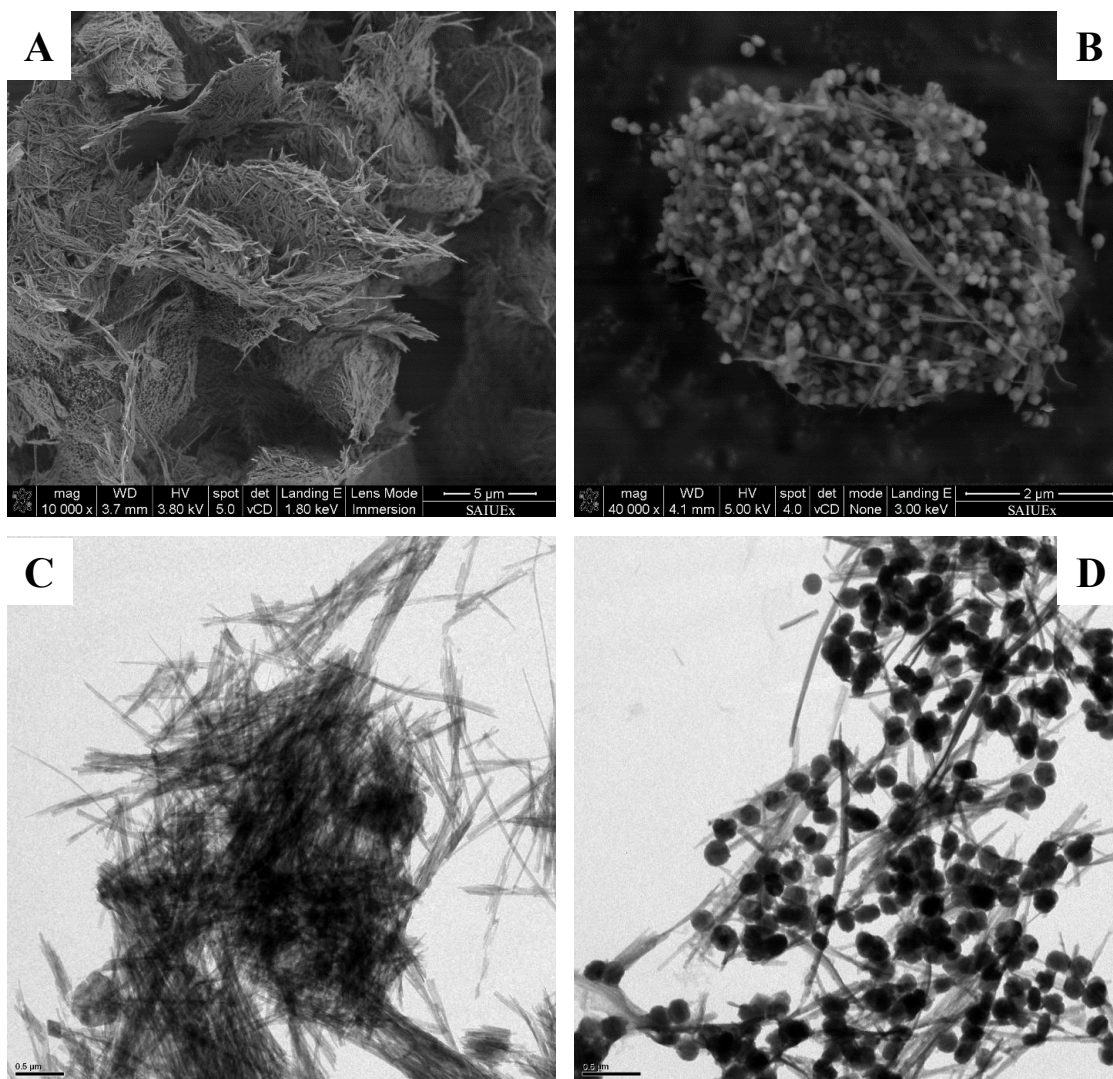


Figure 4: SEM (A, B) and TEM (C, D) images of O-Sep and Zeo-Sep used in IBP adsorption.

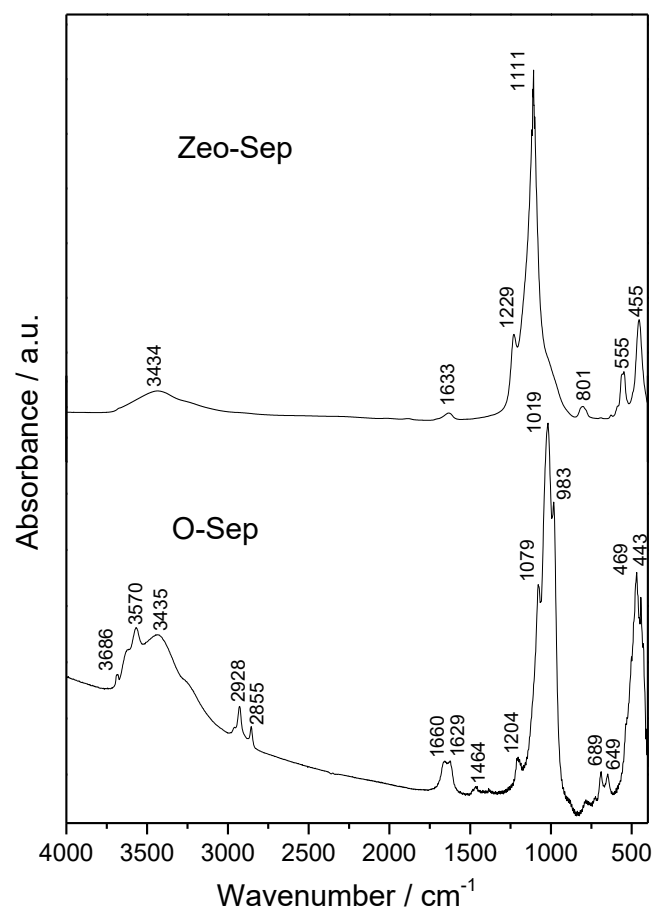


Figure 5: FTIR spectra of O-Sep and Zeo-Sep- heterostructure.

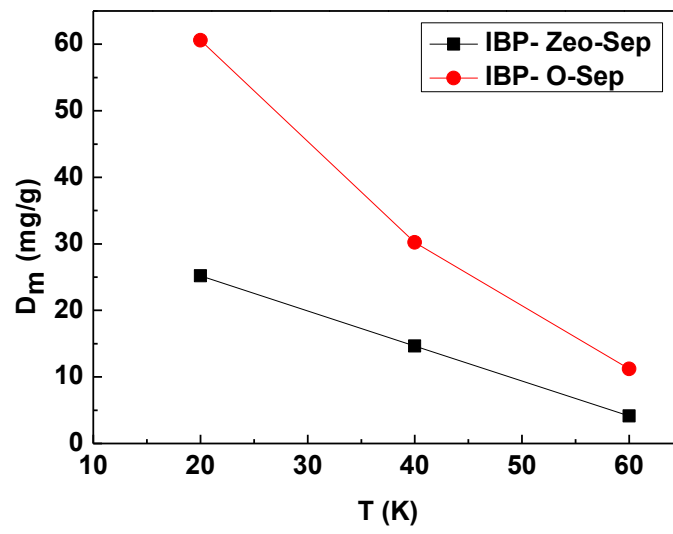


Figure 6: Effect of temperature on the parameter D_m for the adsorption of IBP on Zeo-Sep and O-Sep.

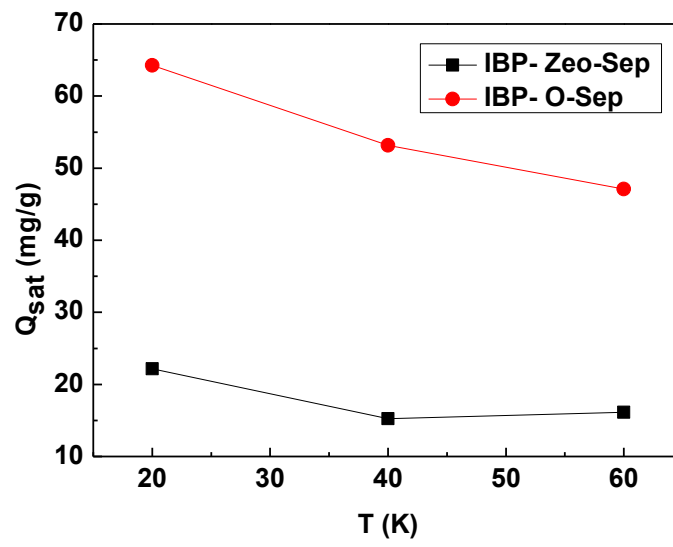


Figure 7: Effect of temperature on the parameter Q_{sat} for the adsorption of IBP on Zeo-Sep and O-Sep.